Unraveling how winds and surface heat fluxes control the Atlantic Ocean's meridional heat transport

Dhruv Bhagtani[1]*, **Andrew McC. Hogg[1]**,
Ryan M. Holmes[2], **and Navid C. Constantinou[1]**

[1]Research School of Earth Sciences and ARC Centre of Excellence for Climate Extremes, Australian
National University, Canberra, ACT, Australia
[2]Australian Bureau of Meteorology, Sydney, NSW, Australia

Key Points:

- We quantify the individual impacts of winds and buoyancy forcing on Atlantic ocean heat transport using flux-forced ocean model simulations
- The circulation response to forcing dominates heat transport initially, while temperature structure changes feed back after several decades
- Heat transport at warm temperatures (the gyre) is sensitive to wind forcing while at cold temperatures it is sensitive to buoyancy forcing

Abstract

The North Atlantic Ocean circulation, fueled by winds and surface buoyancy fluxes, carries 1.25 PettaWatts of heat poleward in the subtropics, and plays an important role in regulating global weather and climate patterns. Using a series of simulations with perturbed surface forcing, we study how winds and surface heat flux gradients affect the Atlantic meridional heat transport. We decompose the Atlantic meridional heat transport into contributions from circulation cells at warm and cold temperatures (resembling a subtropical gyre and the dense overturning circulation respectively), and a mixed circulation that contains water masses traversing both these cells. Variations in wind stress initially alter the amount of heat carried by the warm and mixed cells, but on long time scales (>10 years), changes in the temperature distribution restore the heat transport to equilibrium. Changes in surface buoyancy forcing control the cold cell's circulation, and its associated meridional heat transport, through high-latitude processes.

Plain Language Summary

The Earth gains heat from the sun in the tropics and loses heat near the poles. To maintain a balance, the large-scale circulation in the ocean and the atmosphere must carry heat from the tropics to the poles. Here, we focus on the Atlantic ocean circulation, which is jointly fueled by winds and surface heat and freshwater inputs, and try to understand how this movement of heat poleward is affected by these surface forcings. To do so, we use global ocean model simulations in which we change either winds or surface heat fluxes across the globe, and analyze how the poleward heat transport changes in each set of experiments. We further split the ocean circulation into three components: *(i)* currents flowing near the ocean's surface, *(ii)* currents in the deep ocean, and *(iii)* mixed waters that have the ability to traverse both near-surface and deep ocean currents. We then identify which bit of the circulation carries heat poleward and how they are affected by the forcings. We find that the near-surface ocean currents and their associated poleward heat transport are quick to

---

*142 Mills Road, Acton, 2601, ACT, Australia

Corresponding author: Dhruv Bhagtani, `dhruv.bhagtani@anu.edu.au`

respond to changes in winds, while the deep ocean currents react relatively slowly to changes in surface heat inputs.

1 Introduction

The Atlantic Ocean circulation is steered by a combination of winds and surface buoyancy fluxes and plays a critical role in advecting heat poleward so that the climate system comes to a radiative equilibrium. Modeling studies (Msadek et al., 2013; Stepanov et al., 2016; Liu et al., 2022) and hydrographic surveys (Johns et al., 2011; Srokosz & Bryden, 2015; Trenberth et al., 2019; Frajka-Williams et al., 2019) estimate that the Atlantic Ocean circulation carries around $1.25\,\mathrm{PW}$ ($1\,\mathrm{PW} \equiv 10^{15}\,\mathrm{W}$) of heat poleward in the subtropics. This $1.25\,\mathrm{PW}$ of heat transport is a significant fraction of the $5.5\,\mathrm{PW}$ of heat carried jointly by the ocean and the atmosphere (Masuda, 1988). Changes in the circulation that drives this Atlantic poleward heat transfer are expected due to variations in surface forcing caused by climate change (Mecking & Drijfhout, 2023). Such changes include the meridional shifts in western boundary currents (Gupta et al., 2021) and the response of the meridional overturning to variations in Southern Ocean westerlies (Hogg et al., 2017; Webb et al., 2021). These anticipated changes will have widespread impact on the climate, yet the relative importance of the various mechanisms driving the meridional heat transport (MHT) are not fully understood.

Circulation in the Atlantic Ocean is dominated by two distinct (albeit interconnected) mechanisms. First, cooling, sea ice formation, and convection in the subpolar North Atlantic produces dense water that plays a fundamental role in driving the deep arm (between $1000\,\mathrm{m}$–$3000\,\mathrm{m}$) of the Atlantic Meridional Overturning Circulation (AMOC) (Cessi, 2019). This dense water formation and consequent meridional overturning circulation is thus responsible for northward heat transfer in both hemispheres (Bryan, 1991; Frajka-Williams et al., 2019) and dominates the Atlantic MHT variability (Jones et al., 2023). This northward heat transport in both hemispheres by an overturning circulation is unique to the Atlantic basin (Cessi, 2019). On the other hand, the shallow (upper $\sim 500\,\mathrm{m}$) subtropical gyre confined between 20°N and 40°N carries warm waters poleward via the energetic Gulf Stream, with a relatively colder return flow. This joint circulation in the Atlantic is in contrast to the Pacific Ocean circulation, where dense water formation is not observed and thus the subtropical gyre is primarily responsible for MHT (Navarro-Labastida & Farneti, 2023). The AMOC and the subtropical gyre, and by extension their respective heat transports, are affected differently due to climate change (Fox-Kemper et al., 2021). We, therefore, argue that partitioning of the circulation into overturning and gyre components can reveal dynamical links between surface forcing that drives circulation and the resultant heat transport.

The first attempts to isolate the contributions of the subtropical gyre and the AMOC to the heat transport used Eulerian averaging techniques (Hall & Bryden, 1982; Bryan, 1982). These techniques assume that the heat transport by the AMOC at a given latitude is the vertical integral of the product of a zonally averaged velocity and a zonally averaged temperature, with the residual being the gyre component of the MHT (assuming zero net volume transport at the given latitude). Based on these Eulerian-averaging techniques, Roemmich and Wunsch (1985) and Bryden and Imawaki (2001) designate the AMOC as the primary driver of Atlantic MHT by virtue of the large temperature difference between its warmer, shallow northward branch and the colder, deep equatorward branch. This separation and subsequent analyses are motivated by conventional viewpoints that mechanical forcing (surface winds) primarily drives near-surface horizontal circulation (Sverdrup, 1947; Wunsch & Ferrari, 2004), while surface buoyancy forcing exerts a dominant control on the deep vertical meridional overturning circulation (Stommel & Arons, 1959). However, recent literature points to more interconnected roles of these surface forcings in driving the large-scale ocean circulation (Hogg & Gayen, 2020; Bhagtani et al., 2023), and suggests the need to seek other approaches for MHT partition.

An alternative approach is to partition the ocean circulation based on potential density or temperature. Talley (2003) used a density decomposition to divide the ocean into shallow, intermediate, and deep waters and found similar northward heat contributions of the shallow and deep water masses (that correspond to a gyre and an inter-hemispheric overturning, respectively). Boccaletti et al. (2005) and Greatbatch and Zhai (2007) separated the shallow and deep overturning circulations in latitude–temperature space, and found similar magnitudes of heat transported by the subtropical gyre and the AMOC, in line with Talley (2003). In contrast Xu et al. (2016), using output from numerical models alongside observations from the RAPID array (Cunningham et al., 2007), found that the subtropical gyre carries a net southward heat flux in density space.

The proportion of heat carried by the subtropical gyre and the AMOC is sensitive to the technique employed to partition the two circulations. Given the strongly coupled nature of the two circulations (Burkholder & Lozier, 2014; Berglund et al., 2022), an objective delineation between them may not be possible (Foukal & Chafik, 2022; Johns et al., 2023). The coupling between the AMOC and the gyre is explicitly acknowledged in the decomposition proposed by Ferrari and Ferreira (2011), who extended the latitude–temperature framework of Boccaletti et al. (2005) to include a mixed circulation that captures water masses transiting both the subtropical gyre and the AMOC. Ferrari and Ferreira (2011) found that the mixed circulation carries about 75% of the Atlantic MHT and is sensitive to both winds and diapycnal mixing. Therefore, the mixed cell's MHT is expected to vary due to climate change causing variations in surface forcing (such as the intensification of westerlies predicted in the future (Shaw & Miyawaki, 2024)).

In this paper, we build on the work of Ferrari and Ferreira (2011) to separate the Atlantic circulation in latitude–temperature space into a warm (gyre), cold (AMOC), and a mixed circulation that span temperature classes occupied by both the warm and cold cells. The methodology, described in section 2, is applied to a series of flux-forced global ocean simulations with independently perturbed wind stress or surface heat fluxes (details in section 2.1 and in the work by Bhagtani et al. (2023)). We use these simulations to analyze the influence of surface forcing on the Atlantic MHT carried by the warm, cold, and mixed circulations (results in sections 3.1 and 3.2 respectively) and conclude with a discussion in section 4.

2 Models and methods

2.1 Model setup

We analyze a series of global ocean simulations described by Bhagtani et al. (2023). These simulations use the Modular Ocean Model v5.1 (Griffies, 2012) at a horizontal resolution of 0.25° and with 50 vertical levels. The model is forced using prescribed climatological surface boundary fluxes, obtained from the last 20 years of a 200-year-long equilibrated simulation of the ACCESS-OM2 ocean–sea ice model (Kiss et al., 2020). In reality, surface buoyancy fluxes in the ocean are affected by a variety of physical parameters, such as atmospheric and sea surface temperatures, humidity, surface winds, and radiative fluxes. While our choice of model setup produces higher surface temperature variance in some regions due to no surface heat flux damping, it allows us to eliminate dependencies between surface forcings, thereby enabling us to modify each forcing independent of the other.

We conduct two types of sensitivity experiments: *(i)* variations in global wind stress, and *(ii)* variations in surface meridional heat flux gradients at the subtropical–subpolar boundary in all ocean basins. Each sensitivity experiment is run for 100 years to allow both the surface and the deep circulations to respond to variations in surface forcing; the first 10 and last 50 years of each experiment are analyzed.

A disadvantage of using surface boundary fluxes to force the ocean is that the high-latitude ocean cools very rapidly, which is mitigated by switching on dynamic frazil for-

mation in polar regions. The small heat input associated with the frazil formation slowly increases the sea surface temperatures by $0.15°\text{C decade}^{-1}$. We note that this drift is quite small compared to the applied surface perturbations, and can largely be removed by comparing diagnostics across perturbation experiments (see an expanded discussion on frazil formation in the flux-forced simulations in the paper by Bhagtani et al. (2023)).

2.2 Definition of warm, cold, and mixed cells in latitude–temperature space

The streamfunction Ψ in latitude–temperature space is defined as (see e.g., Ferrari and Ferreira (2011); Holmes et al. (2019)):

$$\Psi(\phi, \theta, t) \stackrel{\text{def}}{=} R \int_{\lambda_w}^{\lambda_e} \int_{-D}^{\eta} v(\lambda, \phi, z, t)\, \mathcal{H}(\theta - \theta_c(\lambda, \phi, z, t)) \cos \phi \, \mathrm{d}z \, \mathrm{d}\lambda, \qquad (1)$$

where R is the Earth's radius, λ is the longitude, ϕ is the latitude, v is the meridional velocity, λ_w and λ_e are the western and eastern extents of the Atlantic basin at a given latitude ϕ, D is the ocean's depth, η is the sea level, $\mathcal{H}$ is the Heaviside function, and θ_c is the conservative temperature (McDougall & Barker, 2011). Here, we compute the streamfunction for temperatures $\theta \in [-2, 60]°\text{C}$ and with a $1°\text{C}$ interval; recomputing (1) with $0.5°\text{C}$ or $2°\text{C}$ intervals gave similar results. Also, we use monthly-averaged velocity and temperature diagnostics to compute the streamfunction, therefore neglecting the small contributions (compared with the size of our heat transport response) of sub-monthly variability to the MHT (Yung & Holmes, 2023).

The streamfunction (1) for the flux-forced control simulation is shown in Fig. 1b. Positive values that occupy the bulk of the temperature space denote clockwise circulation comprising of warmer waters flowing northward and colder waters returning southward. We also observe weak anti-clockwise circulation cells associated with Antarctic Bottom Water at temperatures below $3°\text{C}$ and the Southern Hemisphere subtropical gyre at warm temperatures. We divide the clockwise portion of the streamfunction into a warm (Ψ_{warm}), a cold (Ψ_{cold}), and a mixed (Ψ_{mixed}) circulation cell following Ferrari and Ferreira (2011). The warm cell (enclosed by the red contour in Fig. 1b) represents the subtropical gyre and encloses the peak in the streamfunction at warmer temperatures (=10.1 Sv; red text in Fig. 1b). Similarly, the cold cell (bounded by the blue contour in Fig. 1b) represents the inter-hemispheric AMOC and encloses the peak in the streamfunction at colder temperatures (=21.3 Sv; blue text in Fig. 1b). However, it is clear that a significant proportion of the clockwise circulation transits around both the warm and cold cells. This proportion is captured by the mixed circulation, which is present at all temperatures. We note that this decomposition cannot be used to separate the North Atlantic subpolar gyre from the dense overturning circulation, since the two circulatory features occupy similar temperature ranges. As a result, the decomposition estimates that the entire MHT is carried by the mixed circulation at high latitudes. Therefore, the decomposition by Ferrari and Ferreira (2011) can only be used to separate MHT contributions by the subtropical gyre and the dense overturning circulation.

The strength of the mixed circulation (= 6.3 Sv; black text in Fig. 1b) is quantified as the closed streamfunction contour with the smallest value of Ψ that completely isolates the warm and cold cells. This streamfunction contour separates the warm and cold cells at the saddle point, which corresponds to temperature θ_{saddle} and latitude ϕ_{saddle} (the solid black triangle in Fig. 1b; annotated by green arrow). Once the saddle point has been found, the strength of the warm and cold circulations are computed by subtracting the mixed circulation for regions with $\Psi > \Psi_{\text{mixed}}$ (enclosed by red and blue contours respectively in

Fig. 1b) from the streamfunction Ψ. Specifically,

$$\Psi_{\text{warm}} \overset{\text{def}}{=} \begin{cases} \Psi - \Psi_{\text{mixed}} & \text{if } \Psi > \Psi_{\text{mixed}} \text{ and } \theta \geq \theta_{\text{saddle}}, \\ 0 & \text{otherwise}, \end{cases} \tag{2}$$

$$\Psi_{\text{cold}} \overset{\text{def}}{=} \begin{cases} \Psi - \Psi_{\text{mixed}} & \text{if } \Psi > \Psi_{\text{mixed}} \text{ and } \theta < \theta_{\text{saddle}}, \\ 0 & \text{otherwise}. \end{cases} \tag{3}$$

Following these definitions, the flux-forced control streamfunction in Fig. 1b implies that the mixed circulation strength is 6.3 Sv, the warm (gyre) cell strength is 3.8 Sv and the cold (overturning) cell strength is 15 Sv.

2.3 Heatfunction

One advantage of using a streamfunction defined in temperature–latitude space is that the MHT is easily computed via a cumulative integral in temperature (see e.g., Ferrari and Ferreira (2011)). This defines a *heatfunction*,

$$\text{H}(\phi, \theta, t) \overset{\text{def}}{=} \rho_0 c_p \int_{-2^\circ\text{C}}^{\theta} \Psi(\phi, \theta', t) \, \mathrm{d}\theta', \tag{4}$$

where ρ_0 is the reference density and c_p is the specific heat capacity (both of which are constants in our Boussinesq model simulations that use conservative temperature). The heatfunction (4) is equal to the cumulative MHT for waters colder than θ, and can be used to estimate the MHT for a closed circulation (i.e., a mass-conserving circulation whose heat transport is robustly defined independently of the reference temperature) along an isocontour of the streamfunction Ψ at a given latitude ϕ:

$$\text{MHT}(\phi) = \text{H}(\phi, \theta^{\max}) - \text{H}(\phi, \theta^{\min}), \tag{5}$$

where $\theta^{\min}$ and $\theta^{\max}$ are the minimum and maximum temperatures spanned by the given circulation cell.

The heatfunction for the flux-forced control simulation is shown in Fig. 1e. The heatfunction is mostly positive and increases with temperature, demonstrating the dominant northward heat transport throughout the Atlantic associated with the clockwise circulation in the latitude–temperature plane. The total northward MHT, indicated by the value of the heat function at the maximum temperature, is largest in the subtropics, where clockwise circulation spans the largest temperature range (and thus the cumulative integral is largest). Heatfunction contours that pierce the ocean's surface at latitudes north of 35°N indicate heat loss to the atmosphere (Holmes et al., 2019). Finally, at steady state, the horizontal divergence of the heatfunction contours quantify the air-sea heat exchange.

3 Results

The MHT due to each circulation cell, computed using (5), can vary between the simulations via: *(i)* adjustments in the circulation strength as quantified by the streamfunction Ψ of the given cell, *(ii)* modifications in the temperature range spanned by the circulation, or *(iii)* a combination of both variations in the circulation strength and temperature distribution. These processes occur on different time scales, thus, we examine short (1–10 years) and long (51–100 years) time scale responses of the heat carried meridionally by each cell.

3.1 Wind stress perturbation experiments

We run two perturbation experiments in which we change the global wind stress by a factor of 0.5 and 1.5 (labeled as 0.5×W and 1.5×W respectively) times the control (labeled as CTRL) value. In these experiments, the total surface heat fluxes are held fixed, meaning that
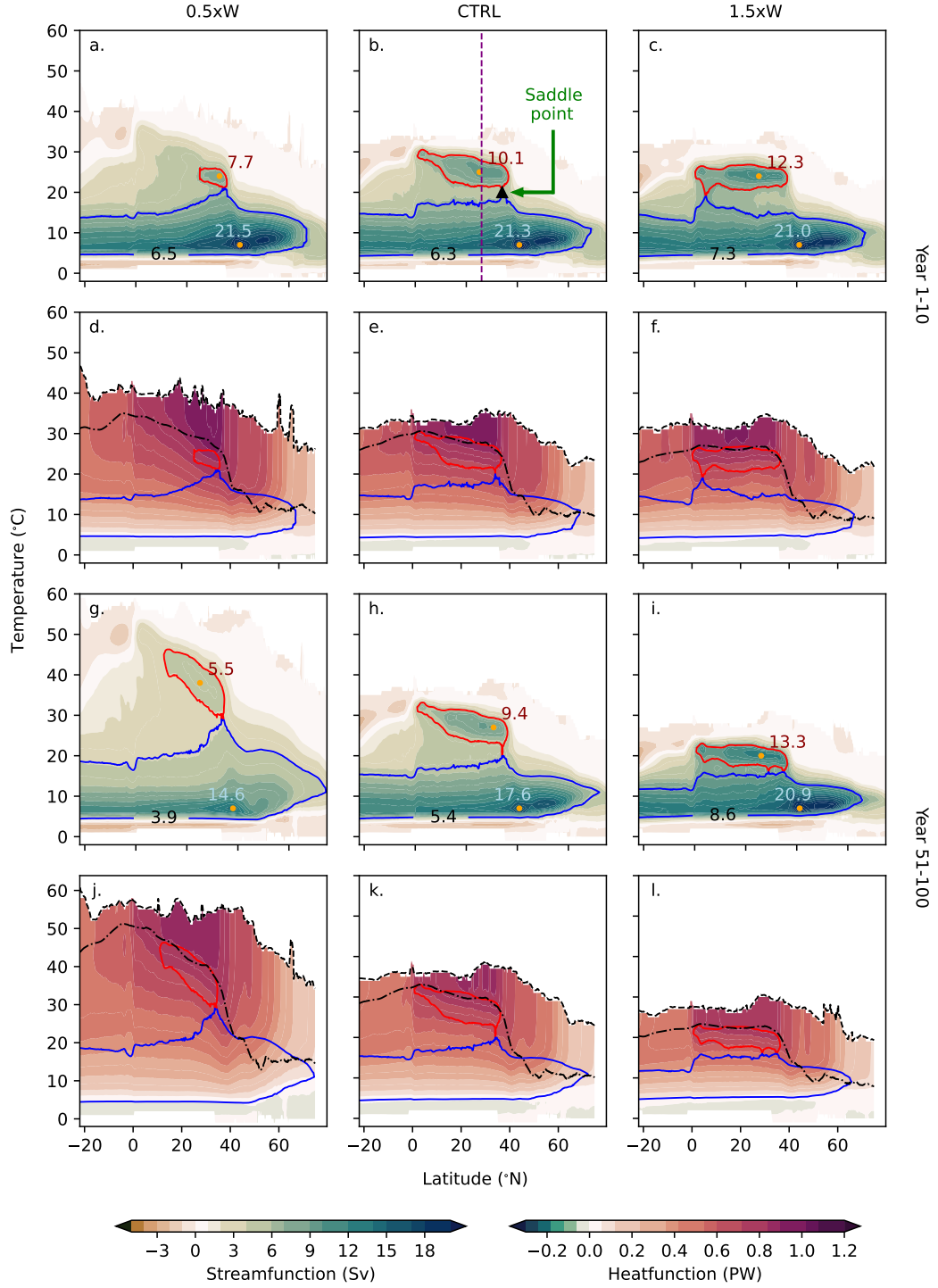
Figure 1. Rows 1 and 3: Streamfunction in latitude–temperature space (left colorbar) calculated from the first 10 years (a-c) and last 50 years (g-i) for the 0.5×W (left column), CTRL (middle column), and 1.5×W (right column) experiments. The strength of the mixed cell (black text), along with the absolute maximum streamfunction enclosed by the warm cell (red text) and the cold cell (blue text) is indicated for each panel. The vertical purple dashed line in panel (b) indicates 26°N which is used to summarize our results. The black solid triangle in panel (b) marks the saddle point temperature θ_{saddle}. Rows 2 and 4: Heatfunction in latitude–temperature space (right colorbar) obtained by cumulatively integrating the streamfunctions in rows 1 and 3 for the first 10 years (d-f) and last 50 years (j-l) for the 0.5×W (left column), CTRL (middle column), and 1.5×W (right column) experiments. The meridional structure of the maximum (dashed black line) and mean (dash-dotted black line) ocean surface temperatures indicate that air-sea heat exchanges at any latitude occur over a range of temperatures.

changes in the net Atlantic MHT are not expected once the simulations reach equilibrium. However, perturbations in wind stress affects each component of the circulation differently, thus, we anticipate a change in the relative contributions of the warm, cold, and mixed circulations to the total Atlantic MHT.

3.1.1 *Initial response*

The circulation strength at warm temperatures scales with the magnitude of wind stress on short time scales (compare the streamfunction within the red contour between Figs. 1a-c). These changes are primarily led by the warm cell (difference between the streamfunction and the black text within the red contour in Figs. 1a-c), with additional smaller changes linked to an increase in the mixed cell's circulation strength with wind stress (black text in Figs. 1a-c). The streamfunction at colder temperatures (enclosed by the blue contour in Figs. 1a-c) is not sensitive to modifications in surface winds in the first 10 years. However, the mixed circulation slightly increases with winds (compare black text between Figs. 1a-c), therefore, the cold cell's circulation (difference between the streamfunction and the mixed cell's circulation strength) is inversely related to the magnitude of wind stress.

In the first 10 years, changes in the circulation of each cell are primarily responsible for changes in the MHT, with little influence from changes in the temperature structure (compare the heatfunction plots between Figs. 1d-f). Therefore, the MHT carried by the warm and mixed cells scales with the magnitude of wind stress, whereas the deep cell's MHT is inversely related to the wind stress strength. These MHT anomalies gradually modify the ocean's meridional thermal structure. For example, variations in the warm and mixed circulations reduce the heat transported poleward in the tropics in the $0.5\times$W experiment (compare the heatfunction plots for 20°S–20°N between Figs. 1d-e), which supports a local convergence of heat fluxes. Consequently, the tropics warm in the $0.5\times$W experiment in the first 10 years (compare the range of temperatures occupied by the zonally–averaged streamfunction in the tropics between Figs. 1a-b). In contrast, the tropics cool in the $1.5\times$W experiment compared to the CTRL (Figs. 1b-c) due to more heat transported poleward by the warm and mixed cells (Figs. 1d-f).

3.1.2 *Long-term response*

On long time scales, variations in the circulation-driven MHT thermally restructures each cell. The temperature distribution anomalies observed in the tropics in the first 10 years (Figs. 1a-c) is amplified in the last 50 years (Figs. 1g-i). Crucially, this temperature restructuring occurs across the entire latitude range, which is likely caused by variations in the amount of heat entering the Atlantic basin at 22°S (heatfunction plots in Figs. 1j-l). Moreover, the temperature restructuring also explains the increase in the peak circulation strength at colder temperatures with wind stress (Figs. 1g-i). Warmer near-surface temperatures at higher latitudes observed in the $0.5\times$W experiment inhibit deep water formation (and the cold cell's strength) in the subpolar North Atlantic. On the contrary, colder near-surface temperatures drive circulation at cold temperatures in the $1.5\times$W experiment on long time scales.

The changes in the temperature structure feed back on the MHT on long time scales (see the temperature dependence on the MHT in (5)). We find that modifications in the ocean's temperature compensate for circulation-driven MHT changes (compare Figs. 1j-l) as we progress towards equilibrium. We expect this compensation between the temperature- and circulation-driven MHT since the total surface heat fluxes are fixed across the three experiments. Each cell in the $0.5\times$W experiment stretches in temperature space, whereas each cell contracts in temperature space in the $1.5\times$W experiment. Such compensation is not observed in the wind perturbation experiments by (Ferrari & Ferreira, 2011), since their surface buoyancy forcing is dependent on the wind stress. To summarize, the total MHT

is kept unchanged in our experiments, but the proportion of heat transported by the warm and mixed cells increases with wind stress, at the expense of the cold cell.

3.2 Surface buoyancy flux contrast experiments

We now examine the circulation and heat transport response to global variations in surface heat fluxes. The anomalous heat flux applied in the subtropics is half that applied in the subpolar and polar regions to ensure a net zero globally-integrated heat flux anomaly (the heat flux pattern is denoted by the heat spectrum at the top of panels (a), (c), (g), and (i) in Fig. 2)). The same anomalous surface meridional heat fluxes are also applied in the Pacific and Indian Oceans (not shown here). Thus, e.g., the $-15\,\mathrm{W\,m^{-2}}$ experiment has $5\,\mathrm{W\,m^{-2}}$ anomalous cooling in the subtropics and $10\,\mathrm{W\,m^{-2}}$ anomalous heating in the subpolar and polar regions.

In these experiments, we envisage variations in the MHT at equilibrium compared to the control, since we apply anomalous meridional heat flux gradients at the ocean's surface. For example, in the reduced buoyancy flux contrast experiments we expect a reduction in the total MHT.

3.2.1 Initial response

In the first 10 years, the main change in circulation is an increase in the peak transport at cold temperatures with the surface heat flux contrast (compare the streamfunction and its peak value in light blue text within the blue contours in Figs. 2a-c). Surface cooling in the subpolar regions in the $+15\,\mathrm{W\,m^{-2}}$ experiment promotes deep water formation, enhancing the transport at colder temperatures. On the other hand, this transport reduces in the $-15\,\mathrm{W\,m^{-2}}$ experiment in response to surface heating. The strength of the mixed circulation slightly increases with the surface heat flux contrast (black text in Figs. 2a-c), while the warm cell is not affected in the first 10 years.

Modifications in the Atlantic MHT stem primarily from changes in the circulation in the first 10 years. Since the circulation strength of the cold and mixed cells increase with the surface heat flux contrast, their associated heat transport also scale similarly (compare the heatfunction plots between Figs. 2d-f). The heatfunction anomalies (Figs. 2d-f) are the largest between 20–50°N, which aligns with the largest anomalies in the cold cell's circulation likely caused by variations in the surface heat fluxes in the high-latitude North Atlantic (Yeager & Danabasoglu, 2014). These localized circulation-driven MHT variations, in turn, affect the ocean's temperature. Increased northward heat transport in the $+15\,\mathrm{W\,m^{-2}}$ experiment between 20–50°N contributes to raising the maximum temperature at these latitudes (compare Figs. 2e-f); the opposite holds for the $-15\,\mathrm{W\,m^{-2}}$ experiment.

3.2.2 Long-term response

On long time scales, the changes in the temperature distribution within each cell in response to circulation-driven MHT variations and anomalous surface heating become clearer. In contrast to the first 10 years where changes in the temperature distribution were localized, here the temperature is modified across all latitudes (see Figs. 2g-i). For example, the maximum temperature reduces in the $-15\,\mathrm{W\,m^{-2}}$ experiment and increases in the $+15\,\mathrm{W\,m^{-2}}$ experiment at all latitudes. Because this temperature change is relatively uniform with latitude, we attribute it to changes in the amount of heat transported into the Atlantic at 22°S (the southernmost extent of the heatfunction plots). This net heat transport into the Atlantic ocean increases with the surface heat flux contrast, and illustrates that the Atlantic MHT responds relatively uniformly rather than only responding where the surface heat flux contrast anomalies are applied. The heat transport at 22°S may be driven by a combination of anomalous surface heat fluxes in the Northern (remote effect) or in the Southern Hemisphere (local effect).
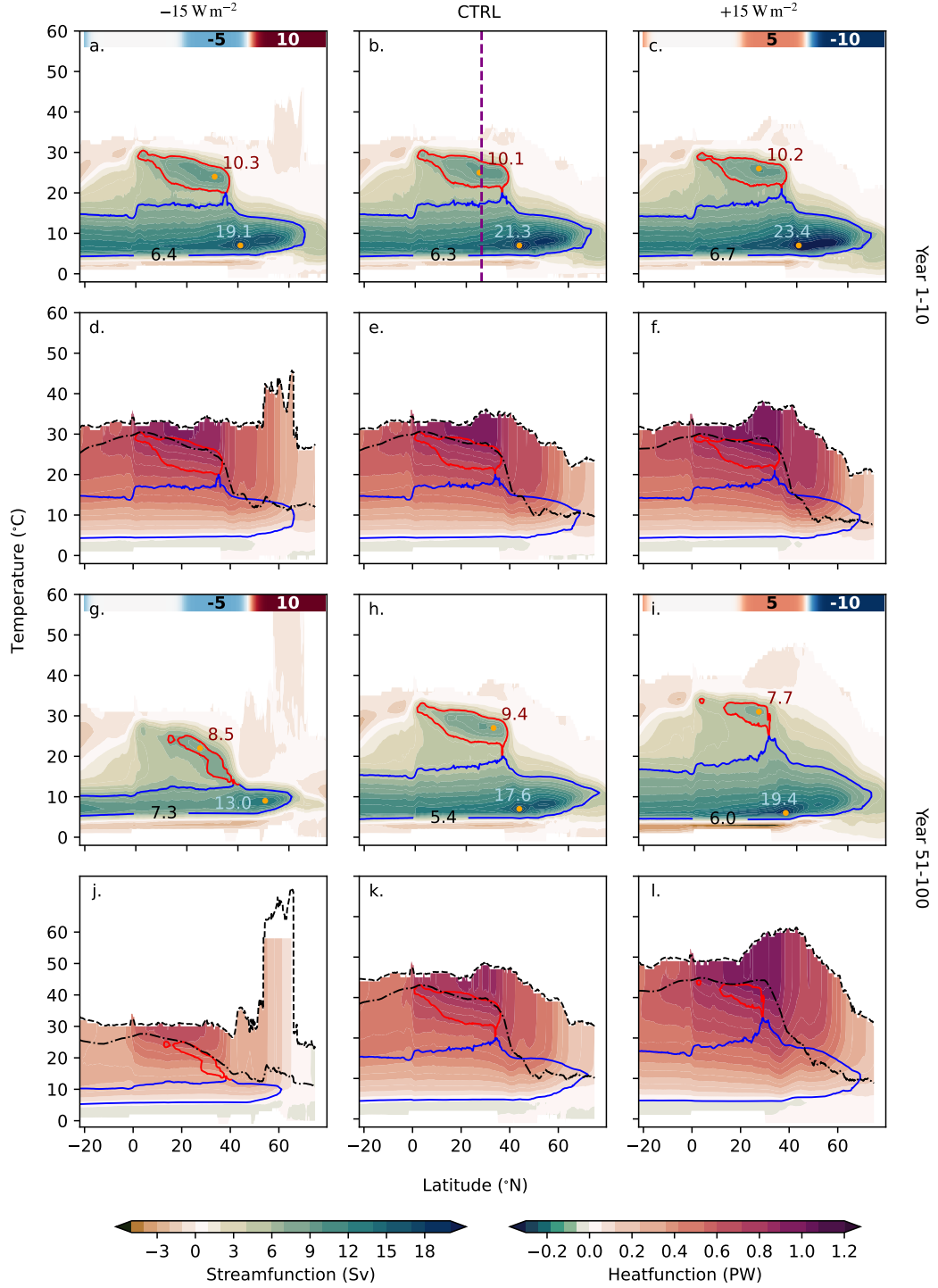
Figure 2. Rows 1 and 3: Streamfunction in latitude–temperature space (left colorbar) calculated from the first 10 years (a-c) and last 50 years (g-l) for the $-15\,\mathrm{W\,m^{-2}}$ (left column), CTRL (middle column), and $+15\,\mathrm{W\,m^{-2}}$ (right column) experiments. The strength of the mixed cell (black text), along with the absolute maximum streamfunction enclosed by the warm (red text) and cold (blue text) cells is indicated for each panel. The vertical purple dashed line in panel (b) indicates $26°$N which is used to summarize our results. The horizontal color spectrum at the top of panels (a), (c), (g), and (i) represents the anomalous surface heat fluxes (in $\mathrm{W\,m^{-2}}$). Rows 2 and 4: Heatfunction (right colorbar) obtained by cumulatively integrating the streamfunctions in temperature indicated in rows 1 and 3 for the first 10 years (d-f) and last 10 years (j-l) of the buoyancy flux contrast perturbation experiments. The meridional structure of the maximum (dashed black line) and mean (dash-dotted black line) ocean surface temperatures indicate that air-sea heat exchanges at any latitude occur over a range of temperatures.

We find that variations in the circulation strength and the temperature distribution act jointly to influence the Atlantic MHT on long time scales (compare the heatfunction plots between Figs. 2j-l). The temperature ranges occupied by the cold cell reduces in the $-15\,\mathrm{W\,m^{-2}}$ experiment and increases in the $+15\,\mathrm{W\,m^{-2}}$ experiment. Moreover, the cold cell's circulation strength reduces in response to anomalous surface heating in the subpolar North Atlantic in the $-15\,\mathrm{W\,m^{-2}}$ experiment, whereas the circulation increases in response to surface cooling in the $+15\,\mathrm{W\,m^{-2}}$ experiment. As a result, the cold cell's MHT scales with the surface heat flux contrast. The mixed cell's MHT also scales similarly, but here, changes in the temperature distribution are primarily responsible for MHT variations as the change in circulation is relatively minor (compare the circulation strength in Figs. 2g-i). We note that the anomalous heating and cooling applied in the Southern Hemisphere (not visible in Fig. 2) may also influence the MHT carried by the cold and mixed cells, especially on long time scales. However, a complete analysis requires separating the response to surface buoyancy flux anomalies applied only in the Northern and Southern Hemispheres respectively, which is beyond the scope of this study. Overall, we find that the meridional heat transport is directly related to the surface heat flux contrast, and the cold and mixed cells jointly drive most of the changes in MHT, with little change in the warm cell transport.

4 Summary and discussion

In this study, we use a series of global ocean–sea ice simulations to quantify the independent effects of wind stress and surface heat fluxes in steering the North Atlantic MHT. We divide the Atlantic circulation into warm (gyre), cold (meridional overturning), and mixed circulations in latitude–temperature space following Ferrari and Ferreira (2011) to understand the sensitivity of each circulation's MHT to varying surface forcing.

We find that the three circulations and their respective MHTs adjust to variations in winds and surface heat fluxes in three ways: *(i)* changes in circulation strength, *(ii)* variations in the temperature distribution of each cell, or *(iii)* a combination of both. We consider the latitude 26°N of the RAPID array (Cunningham et al., 2007) to summarize the changes in circulation, MHT, and the relative contributions of the three cells in both sets of experiments. On short time scales, the circulation strength of the warm and mixed cells increase with wind stress (dashed lines in Fig. 3a). On the other hand, the cold cell's circulation scales with the surface meridional heat flux gradients (blue dashed line, Fig. 3d). Deviations in the circulation drive the MHT on short time scales as significant changes in the temperature structure do not have time to develop. Hence, we observe a direct relationship between the warm cell's MHT and the wind stress (red dashed line, Fig. 3b). The cold cell's MHT increases directly with the surface heat flux contrast (green dashed line, Fig. 3e) likely caused by variations in the surface buoyancy fluxes in the subpolar North Atlantic (Yeager & Danabasoglu, 2014). On long time scales, variations in the circulation-driven MHT thermally restructure each cell (compare the temperature ranges occupied by each cell for the first 10 and last 50 years in Fig. 3c and Fig. 3f). This temperature distribution then feeds back on to the MHT and, together with the variations in circulation, controls the total Atlantic MHT (solid black line in Fig. 3b). The temperature- and circulation-driven MHT variations compensate each other in the wind perturbation experiments, as required to reach equilibrium with a fixed surface heat flux (Fig. 3b). On the other hand, both the temperature- and circulation-driven MHT increase with the surface heat flux gradients, changes which are attributed to the cold and mixed cells (Fig. 3e).

In reality, wind stress and surface buoyancy forcing are strongly coupled and depend on the ocean response itself. In particular, the surface heat flux depends strongly on the ocean's sea surface temperature, which responds dynamically to heat transport changes associated with both winds and surface heat fluxes. Nevertheless, our flux-forced simulations, along with a decomposition of the Atlantic circulation into warm, cold, and mixed cells have provided useful insight and may help understand how MHT may respond to climate change. For example, climate projections suggest a strengthening of zonal winds (Shaw & Miyawaki,
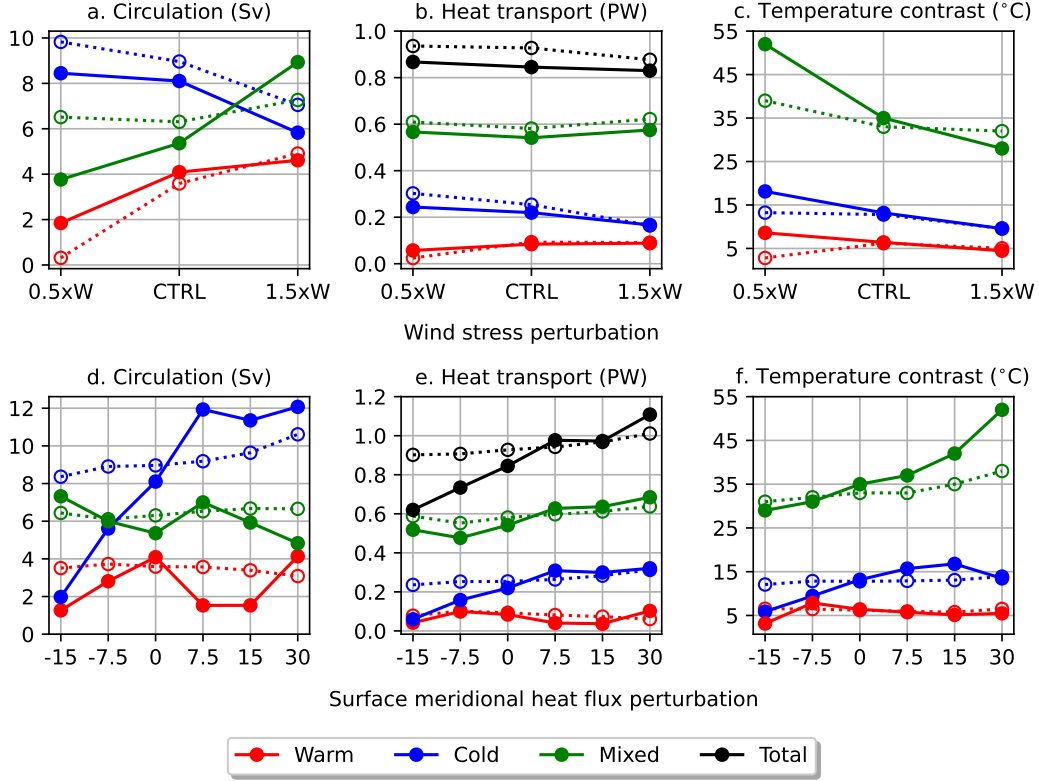
Figure 3. Metrics for meridional heat transport for the first 10 years (dashed lines) and last 50 years (solid lines) for the wind perturbation (top row) and surface meridional heat flux perturbation (bottom row) experiments.

2024). Under such scenarios, our results indicate an increased contribution of the warm cell to northward heat transport, led by a spin up of the subtropical gyre. At the same time, projected melting in the Greenland and the Arctic (Rantanen et al., 2022) are expected to reduce surface buoyancy loss in the North Atlantic leading to a reduction in the MHT carried by the meridional overturning circulation. Whether the mixed circulation's MHT increases or decreases depends on the degree of compensation between the effects of the two surface forcings. The sign of this response will be critical for North Atlantic climate change given that the mixed cell drives approximately 70% of the total Atlantic MHT in our experiments, which is consistent with Ferrari and Ferreira (2011).

Open Research Section

Notebooks used for reproducing the analyses and figures are available at the repository github.com/dhruvbhagtani/Atlantic-meridional-heat-transport-heatfunction. Preprocessed data for the flux-forced simulations is available online at the Zenodo repository doi:10.5281/zenodo.8405008. The modified MOM5 source code for the flux-forced simulations used in this paper is available at github.com/dhruvbhagtani/MOM5.

References

Berglund, S., Döös, K., Groeskamp, S., & McDougall, T. J. (2022). The downward spiralling nature of the North Atlantic subtropical gyre. *Nature Communications*, *13*, 1-9. doi: 10.1038/s41467-022-29607-8

Bhagtani, D., Hogg, A. M., Holmes, R. M., & Constantinou, N. C. (2023). Surface heating steers planetary-scale ocean circulation. *Journal of Physical Oceanography*, *53*, 2375–2391. doi: 10.1175/JPO-D-23-0016.1

Boccaletti, G., Ferrari, R., Adcroft, A., Ferreira, D., & Marshall, J. (2005). The vertical structure of ocean heat transport. *Geophysical Research Letters*, *32*. doi: 10.1029/2005GL022474

Bryan, K. (1982). Seasonal variation in meridional overturning and poleward heat transport in the Atlantic and Pacific oceans: a model study. *Journal of Marine Research*, *40*, 39-53. Retrieved from https://elischolar.library.yale.edu/journal_of_marine_research/1632

Bryan, K. (1991). Poleward heat transport in the ocean. *Tellus A*, *43*, 104-115. doi: 10.1034/j.1600-0870.1991.00009.x

Bryden, H., & Imawaki, S. (2001). Chapter 6.1 Ocean heat transport. In G. Siedler, J. Church, & J. Gould (Eds.), *Ocean circulation and climate* (Vol. 77, p. 455-474). Academic Press. doi: 10.1016/S0074-6142(01)80134-0

Burkholder, K. C., & Lozier, M. S. (2014). Tracing the pathways of the upper limb of the North Atlantic Meridional Overturning Circulation. *Geophysical Research Letters*, *41*, 4254-4260. doi: 10.1002/2014GL060226

Cessi, P. (2019). The global overturning circulation. *Annu. Rev. Mar. Sci*, *11*, 249-270. doi: 10.1146/annurev-marine-010318

Cunningham, S. A., Kanzow, T., Rayner, D., Baringer, M. O., Johns, W. E., Marotzke, J., ... Bryden, H. L. (2007). Temporal variability of the Atlantic Meridional Overturning Circulation at 26.5°N. *Science*, *317*. doi: 10.1126/science.1141304

Ferrari, R., & Ferreira, D. (2011). What processes drive the ocean heat transport? *Ocean Modelling*, *38*, 171-186. doi: 10.1016/j.ocemod.2011.02.013

Foukal, N. P., & Chafik, L. (2022). The AMOC needs a universally-accepted definition. *ESS Open Archive*. doi: 10.1002/essoar.10512765.1

Fox-Kemper, B., Hewitt, H., Xiao, C., Adalgeirsdottir, G., Drijfhout, S., Edwards, T., ... Yu, Y. (2021). Ocean, Cryosphere and Sea Level Change [Book Section]. In V. Masson-Delmotte et al. (Eds.), *Climate Change 2021: The Physical Science Basis. Contribution of Working Group I to the Sixth Assessment Report of the Intergovernmental Panel on Climate Change* (p. 1211–1362). Cambridge, United Kingdom and New York, NY, USA: Cambridge University Press. doi: 10.1017/9781009157896.011

Frajka-Williams, E., Ansorge, I. J., Baehr, J., Bryden, H. L., Chidichimo, M. P., Cunningham, S. A., ... Wilson, C. (2019). Atlantic Meridional Overturning Circu-

lation: Observed transport and variability. *Frontiers in Marine Science*, *6*. doi: 10.3389/fmars.2019.00260

Greatbatch, R. J., & Zhai, X. (2007). The generalized heat function. *Geophysical Research Letters*, *34*. doi: 10.1029/2007GL031427

Griffies, S. M. (2012). *Elements of the Modular Ocean Model (MOM) 2012 release with updates.* Retrieved from www.gfdl.noaa.gov/fms.

Gupta, A. S., Stellema, A., Pontes, G. M., Taschetto, A. S., Vergés, A., & Rossi, V. (2021, 12). Future changes to the upper ocean western boundary currents across two generations of climate models. *Scientific Reports*, *11*. doi: 10.1038/s41598-021-88934-w

Hall, M. M., & Bryden, H. L. (1982). Direct estimates and mechanisms of ocean heat transport. *Deep Sea Research Part A, Oceanographic Research Papers*, *29*, 339-359. doi: 10.1016/0198-0149(82)90099-1

Hogg, A. M., & Gayen, B. (2020, 8). Ocean gyres driven by surface buoyancy forcing. *Geophysical Research Letters*, *47*, 1-10. doi: 10.1029/2020GL088539

Hogg, A. M., Spence, P., Saenko, O. A., & Downes, S. M. (2017). The energetics of Southern Ocean upwelling. *Journal of Physical Oceanography*, *47*, 135-153. doi: 10.1175/JPO-D-16-0176.1

Holmes, R. M., Zika, J. D., Ferrari, R., Thompson, A. F., Newsom, E. R., & England, M. H. (2019). Atlantic ocean heat transport enabled by indo-Pacific heat uptake and mixing. *Geophysical Research Letters*, *46*. doi: 10.1029/2019GL085160

Hoyer, S., & Hamman, J. (2017). xarray: N-D labeled arrays and datasets in Python. *Journal of Open Research Software*, *5*, 1-10.

Johns, W. E., Baringer, M. O., Beal, L. M., Cunningham, S. A., Kanzow, T., Bryden, H. L., . . . Curry, R. (2011). Continuous, array-based estimates of Atlantic ocean heat transport at 26.5°N. *Journal of Climate*, *24*, 2429-2449. doi: 10.1175/2010JCLI3997.1

Johns, W. E., Elipot, S., Smeed, D. A., Moat, B., King, B., Volkov, D. L., & Smith, R. H. (2023). Towards two decades of Atlantic ocean mass and heat transports at 26.5°N. *Philosophical Transactions of the Royal Society A: Mathematical, Physical and Engineering Sciences*, *381*, 20220188. doi: 10.1098/rsta.2022.0188

Jones, S. C., Jiang, S., & Abernathey, R. P. (2023). A new diagnostic for AMOC heat transport applied to the CESM large ensemble. *ESS Open Archive*. doi: 10.22541/essoar.169288706.66225013/v1

Kiss, A. E., Hogg, A. M., Hannah, N., Dias, F. B., Brassington, G. B., Chamberlain, M. A., . . . Zhang, X. (2020, 2). ACCESS-OM2 v1.0: a global ocean–sea ice model at three resolutions. *Geoscientific Model Development*, *13*, 401-442. doi: 10.5194/gmd-13-401-2020

Liu, C., Yang, Y., Liao, X., Cao, N., Liu, J., Ou, N., . . . Zheng, R. (2022). Discrepancies in simulated ocean net surface heat fluxes over the North Atlantic. *Advances in Atmospheric Sciences*, *39*, 1941-1955. doi: 10.1007/s00376-022-1360-7

Masuda, K. (1988). Meridional heat transport by the atmosphere and the ocean: analysis of FGGE data. *Tellus, Series A*, *40 A*, 285-302. doi: 10.3402/tellusa.v40i4.11801

McDougall, T. J., & Barker, P. M. (2011). Getting started TEOS-10 and the Gibbs Seawater (GSW) oceanographic toolbox. *SCOR/IAPSO WG*, *127*, 1–28.

Mecking, J. V., & Drijfhout, S. S. (2023). The decrease in ocean heat transport in response to global warming. *Nature Climate Change*, *13*, 1229-1236.

Msadek, R., Johns, W. E., Yeager, S. G., Danabasoglu, G., Delworth, T. L., & Rosati, A. (2013). The Atlantic meridional heat transport at 26.5°N and its relationship with the MOC in the RAPID array and the GFDL and NCAR coupled models. *Journal of Climate*, *26*, 4335-4356. doi: 10.1175/JCLI-D-12-00081.1

Navarro-Labastida, R. G., & Farneti, R. (2023). The role of shallow and deep circulations in the tropical Pacific ocean heat budget. *Frontiers in Marine Science*, *10*. doi: 10.3389/fmars.2023.1208052

Rantanen, M., Karpechko, A. Y., Lipponen, A., Nordling, K., Hyvärinen, O., Ruosteenoja, K., . . . Laaksonen, A. (2022). The Arctic has warmed nearly four times faster than

the globe since 1979. *Communications Earth & Environment*, *3*, 168. doi: 10.1038/ s43247-022-00498-3

Rocklin, M. (2015). Dask: Parallel Computation with Blocked algorithms and Task Scheduling. In K. Huff & J. Bergstra (Eds.), (p. 130-136). Proceedings of the 14th Python in Science Conference. doi: 10.25080/Majora-7b98e3ed-013

Roemmich, D., & Wunsch, C. (1985). Two transAtlantic sections: meridional circulation and heat flux in the subtropical North Atlantic ocean. *Deep Sea Research Part A, Oceanographic Research Papers*, *32*, 619-664. doi: 10.1016/0198-0149(85)90070-6

Shaw, T. A., & Miyawaki, O. (2024). Fast upper-level jet stream winds get faster under climate change. *Nature Climate Change*, *14*, 61-67. doi: 10.1038/s41558-023-01884-1

Srokosz, M. A., & Bryden, H. L. (2015). Observing the Atlantic Meridional Overturning Circulation yields a decade of inevitable surprises. *Science*, *348*, 1255575. doi: 10 .1126/science.1255575

Stepanov, V. N., Iovino, D., Masina, S., Storto, A., & Cipollone, A. (2016). Methods of calculation of the Atlantic meridional heat and volume transports from ocean models at 26.5°N. *Journal of Geophysical Research: Oceans*, *121*. doi: 10.1002/2015JC011007

Stommel, H., & Arons, A. B. (1959). On the abyssal circulation of the world ocean— I. Stationary planetary flow patterns on a sphere. *Deep Sea Research (1953)*, *6*, 217-233. doi: 10.1016/0146-6313(59)90065-6

Sverdrup, H. U. (1947). Wind-driven currents in a baroclinic ocean; with application to the equatorial currents of the eastern Pacific. *Proceedings of the National Academy of Sciences*, *33*, 318-326. doi: 10.1073/pnas.33.11.318

Talley, L. D. (2003). Shallow, intermediate, and deep overturning components of the global heat budget. *Journal of Physical Oceanography*, *33*, 530-560. doi: 10.1175/ 1520-0485(2003)033⟨0530:SIADOC⟩2.0.CO;2

Trenberth, K. E., Zhang, Y., Fasullo, J. T., & Cheng, L. (2019). Observation-based estimates of global and basin ocean meridional heat transport time series. *Journal of Climate*, *32*, 4567-4583. doi: 10.1175/JCLI-D-18-0872.1

Webb, D. J., Spence, P., Holmes, R. M., & England, M. H. (2021). Planetary-wave-induced strengthening of the AMOC forced by poleward intensified southern hemisphere westerly winds. *Journal of Climate*, *34*, 7073–7090. doi: 10.1175/JCLI-D-20-0858.1

Wunsch, C., & Ferrari, R. (2004). Vertical mixing, energy, and the general circulation of the oceans. *Annual Review of Fluid Mechanics*, *36*, 281-314. doi: 10.1146/annurev .fluid.36.050802.122121

Xu, X., Rhines, P. B., & Chassignet, E. P. (2016). Temperature-salinity structure of the North Atlantic circulation and associated heat and freshwater transports. *Journal of Climate*, *29*, 7723-7742. doi: 10.1175/JCLI-D-15-0798.1

Yeager, S., & Danabasoglu, G. (2014). The origins of late-twentieth-century variations in the large-scale North Atlantic circulation. *Journal of Climate*, *27*, 3222-3247. doi: 10.1175/JCLI-D-13-00125.1

Yung, C. K., & Holmes, R. M. (2023). On the contribution of transient diabatic processes to ocean heat transport and temperature variability. *Journal of Physical Oceanography*. doi: 10.1175/JPO-D-23-0046.1